Available online at www.sciencedirect.com
SCIENCE DIRECT
Journal of Solid State Chemistry 179 (2006) 1707–1719
JOURNAL OF SOLID STATE CHEMISTRY
www.elsevier.com/locate/jssc

$CuAl_2$ revisited: Composition, crystal structure, chemical bonding, compressibility and Raman spectroscopy

Yuri Grin[a,*], Frank R. Wagner[a], Marc Armbrüster[a], Miroslav Kohout[a], Andreas Leithe-Jasper[a], Ulrich Schwarz[a], Ulrich Wedig[b], Hans Georg von Schnering[b]

[a] *Max-Planck-Institut für Chemische Physik fester Stoffe, Nöthnitzer Straße 40, 01187 Dresden, Germany*
[b] *Max-Planck-Institut für Festkörperforschung, Heisenbergstr. 1, 70569 Stuttgart, Germany*

Received 4 January 2006; received in revised form 27 February 2006; accepted 5 March 2006
Available online 13 March 2006

Abstract

The structure of $CuAl_2$ is usually described as a framework of base condensed tetragonal antiprisms [$CuAl_{8/4}$]. The appropriate symmetry governed periodic nodal surface (PNS) divides the space of the structure into two labyrinths. All atoms are located in one labyrinth, whereas the second labyrinth seems to be 'empty'. The bonding of the $CuAl_2$ structure was analyzed by the electron localization function (ELF), crystal orbital Hamiltonian population (COHP) analysis and Raman spectroscopy. From the ELF representation it is seen, that the 'empty' labyrinth is in fact the place of important covalent interactions. ELF, COHP in combination with high-pressure X-ray diffraction and Raman spectroscopy show that the $CuAl_2$ structure is described best as a network built of interpenetrating graphite-like nets of three-bonded aluminum atoms with the copper atoms inside the tetragonal-antiprismatic cavities.

Keywords: $CuAl_2$; Chemical bonding; Raman spectroscopy; ELF; PNS

1. Introduction

$CuAl_2$, the aluminum-rich compound in the binary system Cu–Al, was first reported by Friauf [1]. The relatively simple structural motif appears not only in many representatives of the $CuAl_2$ structure type and its branches but also in more complex structures [2].

From the analysis of geometrical characteristics (unit cell parameters, interatomic distances), three ways to describe the $CuAl_2$ structure can be found in literature. According to Kripiakevich [2] and Schubert [3], the structure is built of piles of condensed [$CuAl_8$] square antiprisms along [001] (Fig. 1, top). The antiprisms are formed by stacking of 3^2434 aluminum nets along [001] which are centered by the half-occupied 4^4 nets of copper [4]. Consideration of the two shortest Al–Al distances leads to the description as a system of interpenetrating graphite-like aluminum 6^3 nets with copper atoms in the channels between the nets (Fig. 1, middle) as shown by Nowotny and Schubert [5]. Further on [6–8] the whole aluminum part of the structure was described as a network built of *tetraederstern* [3] clusters (Fig. 1, bottom).

De facto, based on the different geometrical interpretations, each description pronounces one distinguished interaction between the atoms in the structure, namely Cu–Al in the first case or Al–Al in both others. A detailed quantum chemical bonding analysis was not done up to now. Band structure calculations were performed for $CuAl_2$ only for explanation of some frequencies in the experimentally measured de Haas–van Alphen effect [9]. For the related structure of $PdGa_5$ (with similar tetragonal antiprismatic environment for Pd atoms), the covalent bonding between the gallium atoms of the neighboring antiprisms was shown using electron localization function (ELF) [10]. All this was the reason for performing the investigation of the chemical bonding in $CuAl_2$ described in the present work.

*Corresponding author. Fax: +49 351 46 46 40 02.
E-mail address: grin@cpfs.mpg.de (Y. Grin).

0022-4596/$ - see front matter © 2006 Elsevier Inc. All rights reserved.
doi:10.1016/j.jssc.2006.03.006

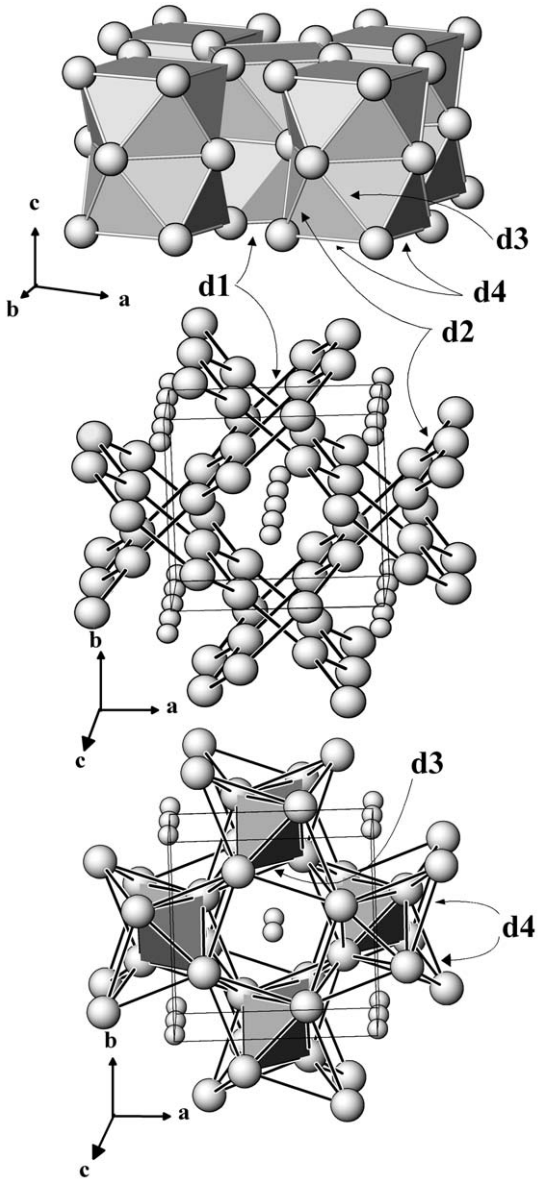

Fig. 1. Three different ways to describe the $CuAl_2$ structure. Cu—small spheres, Al—large spheres.

2. Experimental

2.1. Synthesis

A sample with nominal composition $Cu_{0.3202}Al_{0.6798}$ was prepared by arc melting metal pieces (Al rods, mass fraction 99.9999% and Cu foil, mass fraction 99.99%) on a water-cooled copper hearth under a protective atmosphere of Ti-gettered argon. To ensure homogeneity the ingot was then molten in a water-cooled crucible (Hukin crucible) by inductive HF heating. This procedure was followed by casting the melt into a cylindrical copper mold (8 mm diameter and 60 mm length) which has been mounted on the bottom of the cold crucible. The cylindrical bars were then placed into alumina crucibles of appropriate dimensions and subjected to a modified Bridgman method of crystal growth. The crucible was kept stationary under a protective atmosphere of flowing argon gas during the experiment. The growth process was carried out at 675 °C by slowly moving the furnace upward (2 mm/h), thus subjecting the sample to a thermal gradient. This enabled directed crystallization from the bottom to the top of the crucible. After cooling to room temperature, the crystalline, silvery rods with metallic luster were separated from the crucibles. From metallographical investigation, the rods consisted of relatively large single crystalline grains up to 250 mm^3.

For the investigation of the homogeneity range of $CuAl_2$, two samples with composition $Cu_{20}Al_{80}$ (sample I) and $Cu_{40}Al_{60}$ (sample II) have been prepared by arc-melting the weighted elements (Cu wire, mass fraction 99.99%, and Al granules, mass fraction 99.99%). Subsequently, the samples were sealed in evacuated quartz glass ampoules and annealed at 500 °C for 5 weeks. Afterwards, they were quenched in water to ambient temperature. Powder diffraction patterns were recorded on filings of sample I re-annealed at 500 °C and on powdered sample II.

2.2. Chemical analysis

Chemical analysis was performed locally by the EDXS (scanning electron microscope Philips SX 30) and the WDXS (EPMA CAMECA SX 100; elemental Cu, Al, and later, $Cu_{0.975}Al_2$ as standards) methods. Additionally, selected pieces of the single-phase material were analyzed by ICP MS (PQ ExCell, TJASolutions). Oxygen and nitrogen analysis was performed with the carrier-gas hot-extraction method (TC-436 DR, LECO).

2.3. Thermal analysis

Careful DSC measurements were performed on the single-phase material. A sample of 18.6 mg mass was heated to 450 °C with a heating rate of 10 °C/min in a Netzsch DSC 204 system.

2.4. X-ray diffraction experiments and structure determination

Powder diffraction patterns were measured with a Huber G670 image plate camera ($CuK_{\alpha 1}$ radiation, $\lambda = 1.54056$ Å, high-purity germanium with $a = 5.65752$ Å as the internal standard). Lattice parameters were refined using diffraction angles of 33 reflections. All crystallographic calculations on powder data (XRD profile deconvolution, refinement of the lattice parameters) were performed by means of the Windows version of the Crystal Structure Determination program package (WinCSD) [11]. For single-crystal diffraction experiments, a small piece of the middle part of the rod was used. The X-ray diffraction data were collected with an R-AXIS RAPID diffraction system (Weissenberg setup, image plate detector, graphite monochromator, Mo$K\alpha$ radiation, $\lambda = 0.71069$ Å). For more

Table 1
Crystallographic data for $CuAl_2$

Composition	$CuAl_2$
Crystal size	$0.06 \times 0.06 \times 0.06\,mm^3$
Crystal system	Tetragonal
Space group	$I4/mcm$
Unit cell parameters (powder data)	$a = 6.0637(2)$ Å
	$c = 4.8736(3)$ Å
Volume	$179.19(1)$ Å^3
Z	4
Density (calculated)	$4.36\,g/cm^3$
Wavelength	Mo$K\alpha$, $\lambda = 0.71073$ Å
Absorption coefficient	$12.585\,mm^{-1}$
$F(000)$	220
2θ range	9.5°–126°
Indices ranges	$-15 \leqslant h \leqslant 15$, $-10 \leqslant k \leqslant 10$, $-12 \leqslant l \leqslant 12$
Reflections measured	840
Symmetry independent reflections	416 [$R_{int} = 0.021$]
Completeness of data	97.9%
Refinement method	Full-matrix least-squares on F^2
Data/restraints/parameters	416/0/8
Goodness-of-fit	1.189
Reliability factors [$I > 2\sigma(I)$]	$R_1 = 0.040$, w$R_2 = 0.104$
Reliability factors (all data)	$R_1 = 0.051$, w$R_2 = 0.137$
Extinction coefficient	0.26(3)
Largest diff. peak and hole	2.8 and $-3.5\,e$Å^{-3}

Table 2
Atomic coordinates, equivalent isotropic and anisotropic displacement parameters (in Å^2) for $CuAl_2$

Atom	Site	x	y	z	U_{eq}	
Cu	4a	0	0	$\frac{1}{4}$	0.010(1)	
Al	8h	0.1586(1)	$x + \frac{1}{2}$	0	0.012(1)	
	U_{11}	U_{22}	U_{33}	U_{23}	U_{13}	U_{12}
Cu	0.011(1)	U_{11}	0.007(1)	0	0	0
Al	0.012(1)	U_{11}	0.012(1)	0	0	0

U_{eq} is defined as one third of the trace of the orthogonalized U_{ij} tensor.

information about the data collection, see Table 1. The structure was solved and refined with the SHELXL-97 software [12]. Final values of atomic coordinates and displacement parameters are listed in Table 2. The according residuals are presented in Table 1.

2.5. Raman spectroscopy

The measurements were performed with a LabRam System 010 (Jobin Yvon) in backscattering mode. The setup, equipped with a microscope (objective 100×) and additional filters for low-frequency performance, used the He–Ne 633 nm line with 15 mW as excitation source. For powder measurements, fine-ground powder (~20 μm grain size) was pressed to a pellet in order to reduce the thermal sensitivity. Nevertheless it was necessary to weaken the laser beam for all measurements to 4 mW to avoid decomposition of the material.

To perform the single-crystal measurements, an irregular single-crystalline piece of $CuAl_2$ was mounted on a goniometer head and oriented by X-ray diffraction (Weissenberg- and Laue-techniques). After alignment better than 0.3° along each crystallographic axis, the goniometer head was mounted in the spectrometer. A $\lambda/2$ plate was placed into the beam before and an analyzer was located after the sample. For the different single-crystal experiments, the polarization is given in Porto's notation [13]. In the case of $CuAl_2$, the x, y and z directions are parallel to the crystallographic axes a, b and c, respectively. To verify the Raman signal observed, the Stokes and anti-Stokes modes have been recorded.

2.6. High-pressure X-ray powder diffraction

The high-pressure diffraction experiments were performed using synchrotron radiation at ID9 beamline at the ESRF ($\lambda = 0.4171$ Å). Pressure was applied to the sample by a diamond anvil cell with beryllium backing plates, which allow recording of complete diffraction rings. The sample was placed in a tungsten gasket to reduce the number of gasket reflections. Paraffin was used as pressure transmitting medium and the pressure was calibrated by the ruby scale [14,15]. After masking the gasket rings and reflections due to the diamonds, the pattern was integrated with the program Fit2D [16]. For the determination of the peak positions, indexing and refinement of the cell parameters the software WinCSD [11] was employed.

3. Quantum chemical procedure

The electronic structure of $CuAl_2$ was calculated using the local density functional approach (LDA) as implemented in the Tight-Binding-LMTO program package of Andersen et al. [17] with exchange correlation potential according to von Barth and Hedin [18]. The radial scalar-relativistic Dirac equation was solved to get the partial waves. The calculation within the atomic sphere approximation (ASA) includes corrections from the neglect of the interstitial regions and the partial waves of higher order [19]. The following radii of the muffin tin spheres were used: $r(Cu) = 1.42$ Å, $r(Al) = 1.58$ Å, $r(E) = 0.57$ Å. The basis set consisted of the Cu (4s, 4p, 3d), Al (3s, 3p) LMTOs; Al (3d) orbitals were downfolded [20].

Crystal Orbital Hamiltonian Populations (COHPs) were calculated according to [21] with a special module implemented into the TB-LMTO-ASA program package [22].

Within the TB-LMTO-ASA code the ELF was evaluated according to [23–25] using all orbitals (i.e., core and valence orbitals) of the converged SCF solution. Applying the topological procedure proposed by Bader for the electron density [26] the whole three-dimensional field of ELF values $\eta(\mathbf{r})$ can be divided into the basins of core and

bonding attractors. Integration of the electron density within these basins gives the number of electrons assigned to the according attractor (electron count) and has been suggested to be related to the bond multiplicity [27]. Further information of the calculation and interpretation is given in [10,28,29].

ELF distributions $\eta(\mathbf{r})$ were additionally calculated with the program TOPOND98 [30] based on CRYSTAL98 [31] using optimized all-electron valence triple-zeta (Cu) and valence double-zeta (Al) basis sets, and with the first-principles, all-electron, full-potential local orbital minimal basis method (FPLO) [32,33]. ELF calculations on molecules were performed using the program DGrid [34] interface to the ADF [35] quantum chemical program system. ADF was used to calculate the DFT wavefunction (within LDA) for diatomic molecules using triple-zeta basis sets (Slater functions) with two sets of polarization functions ("TZ2P") for Cu and Al.

The topological analysis of $\eta(\mathbf{r})$ (determination of critical points, evaluation of basins) and the electron density integration inside the basins was done numerically throughout this paper using an adequately fine mesh ($\Delta \approx 0.03$ Å) with the program system Basin [36]. The basin interconnection points (bips) [28] are located on the separating surfaces between touching basins. Topologically they are saddle points, which occur where the ELF reaches its highest value within the contact surface between two or more basins. Analyzing the topology of $\eta(\mathbf{r})$ one is sometimes faced with the occurrence of $\eta(\mathbf{r})$-flat basins in spatial regions of chemical interest. An $\eta(\mathbf{r})$-flat basin is not flat in position space, but in $\eta(\mathbf{r})$-space, which means that the numerical difference between the attractor and the bip value, $\eta(\mathbf{r}_{att})-\eta(\mathbf{r}_{bip})$, is very small. For these situations two different cases can be distinguished depending the estimated accuracy $\delta\eta$ of the calculation: (i) if $\eta(\mathbf{r}_{att})-\eta(\mathbf{r}_{bip})<\delta\eta$ then a significant distinction between those basins can no longer be done and a super basin *cwn* [37] containing both should be formed; (ii) if $\eta(\mathbf{r}_{att})-\eta(\mathbf{r}_{bip})>\delta\eta$ we attribute physical/chemical significance to basin of $\mathbf{r}_{att}$, although it may be difficult to achieve convergence of the calculation with respect to the location of the bip and the size of this basin. This latter scenario is met in our calculations for $CuAl_2$ using CRYSTAL98/TOPOND, where the basin shapes and electronic basin populations of two basin types could not be determined satisfactorily due to still strong dependence on the basis set, although the energetic convergence (with respect to basis set alterations) was already quite good. Calculation schemes using numerical, self-adapting basis sets, as, e.g. the LMTO-ASA method, do not suffer from this kind of problems and we therefore discuss the LMTO-ASA results explicitly and compare with CRYSTAL/TOPOND or FPLO results, where it is convenient to do. For our calculations presented hereafter we used $\delta\eta = 0.005$ for the LMTO-ASA and the CRYSTAL98/TOPOND calculations.

4. Results and discussion

4.1. Composition and homogeneity range

The EDX analysis of the rod-like samples after synthesis did not show any other elements than Cu and Al in the sample. The elemental trace analysis with ICP MS did not detect any metallic elements besides copper and aluminum within the detection limit of 125 ppm. Analysis of the oxygen and nitrogen content did not reveal occurrence of these elements within the detection limits of 0.01% and 0.05%, respectively. The total composition of the single crystals was found to be $Cu_{0.975(8)}Al_2$.

A theoretical investigation of $CuAl_2$ [38] predicted a low-temperature modification with a tetragonally distorted CaF_2 structure formed at 150 °C. Our careful DSC measurements with subsequent X-ray powder diffraction did not give any hints to a structural phase transition in the temperature region from 25 to 450 °C. The compound decomposes peritectically at 589 °C, which correlates well with the literature data (592 °C [39]).

WDXS analysis of the majority phase in the samples I and II revealed compositions $Cu_{32.4(2)}Al_{67.6(2)}$ and $Cu_{33.57(4)}Al_{66.43(4)}$, respectively. Thus the homogeneity range of $CuAl_2$ is approximately 1 at.-% at 500 °C. From the powder diffraction, the corresponding lattice parameters were determined to be $a_I = 6.0708(2)$ Å, $c_I = 4.8802(3)$ Å and $a_{II} = 6.0618(3)$ Å, $c_{II} = 4.8736(3)$ Å which confirms a small homogeneity range of the compound [39,40]. We note the copper deficiency in the whole homogeneity range (i.e. the formula should be written as $Cu_{1-x}Al_2$) and, especially, around the nominal composition, where the single crystals were grown.

4.2. Crystal structure of $CuAl_2$

The crystal structure reported in the literature was confirmed. The obtained crystallographic information (Tables 1 and 2) is in good agreement with the previous results [41]: space group $I4/mcm$ (no. 140); $a = 6.067(1)$ Å, $c = 4.877(1)$ Å, $c/a = 0.8039$, $Z = 4$; Cu at position 4*a*; Al at position 8*h* with $x(\mathrm{Al}) = 0.1581(1)$. From the difference in the atomic mass, one would expect smaller values for the displacement parameter of cupper in comparison with one for aluminum. In fact, the displacement parameters for copper and aluminum atoms are practically equal, suggesting that not only the thermal motion is contributing to the diffraction pattern, but also e.g., small deficiency on the copper position. This is in agreement with the copper-poor composition of the single crystals found with WDXS and ICP AOS analyses. Nevertheless, an attempt to refine the occupancy factor for the copper position (SOF = 0.98(1)) did not lead to the clear confirmation of the tiny deviation from the stoichiometric composition. The final answer to this question could be given on basis of the NMR data [42].

The *intra-polyhedral* distances in the $[CuAl_{8/4}]$ square antiprism are (cf. also Fig. 1): $d5(\mathrm{Cu–Al}) = 2.5874(5)$ Å

(8×); $d2$(Al–Al) = 2.8975(5) Å (4×), $d3$(Al–Al) = 3.1044 (5) Å (8×) and $d4$(Al–Al) = 3.2281(6) Å (8×). The average value is $\bar{d}$(Al−Al) = 3.1125 with the ratio $\bar{d}$(Al−Al)/d(Cu−Al) = 1.203. The shortest *inter-polyhedral* distances are in the Al_2 dumb-bells and between the copper atoms along [001]: $d1$(Al–Al) = 2.7201(9) Å and d(Cu–Cu) = 2.4368(1) Å, respectively. The above-mentioned interpenetrating graphite-like aluminum nets are formed by $d1$ and $d2$ (1× and 2× per Al). For comparison, the interatomic distances in the structures of the elements are d(Al–Al) = 2.864 Å (12×) and d(Cu–Cu) = 2.556 Å (12×).

The connection pattern defined by the site symmetry of the atomic positions (422 for Cu in 4*a* and *m*2*m* for Al in 8*h*) strongly restricts the adjustment of appropriate interatomic distances and results in the observed distortion of the square antiprism (SAP) around the copper atom: $d2 \neq d3 \neq d4$ and $h < h'$. An ideal SAP [$CuAl_8$] with the point symmetry $\bar{4}$ is characterized by the ratio

$$Q' = \bar{d}(\mathrm{Al-Al})/d5(\mathrm{Cu-Al}) = (2\sqrt{8}/(1+\sqrt{8}))^{1/2} = 1.2156$$

and by the height

$$h' = 2^{-1/4} \times \bar{d}(\mathrm{Al-Al}) = 0.8409 \times \bar{d}(\mathrm{Al-Al}).$$

The *condensation* of these ideal SAPs to form the $CuAl_{8/4}$ network of the $CuAl_2$ structure requires $x'(\mathrm{Al}) = (4+\sqrt{8})^{-1} = 0.14645$ [6,8] which yields $c'/a' = \sqrt{2}/(1+\sqrt{2})^{1/2} = 0.9102$. From the experimental volume $V = 179.2\ \text{Å}^3$ follows: $a' = 5.8175$ Å, $c' = 5.2950$ Å, d'(Cu–Al) = 2.5901 Å, $\bar{d}'$ (Al–Al) = 3.1485 Å and d'(Cu–Cu) = 2.6475 Å, but the resulting *inter-polyhedral* distance $d1'$(Al–Al) = $(\sqrt{2}-1)a' = 2.4096$ Å would be much too short. On the other hand, the formation of an equidistant 3^2434 aluminum net requires $x'(\mathrm{Al}) = 0.1830$ [4,6,8] resulting in $d1' = d4' = 3.0112$ Å, $d2' = 2.8678$ Å, $d3' = 3.4018$ Å and d'(Cu–Al) = 2.5073 Å in the same unit cell. In this case, the *intra-polyhedral* $d2'$(Al–Al) would be too short as well as d'(Cu–Al) would be compressed. A comparison of the distances derived above with the experimental values reveals the latter to be a 'reasonable' compromise between both restrictions described above.

The covalent single bond lengths are 2.50 Å (Al) and 2.35 Å (Cu), respectively. The single bond lengths were derived by Pauling from the structures of the metallic elements [43] and they are well established in the structural chemistry of copper and aluminum compounds. The analysis of the $CuAl_2$ structure in terms of the Pauling bond order (PBO) [43] yields in PBO($d5$) = 0.54; PBO(Cu–Cu) = 0.72; PBO($d1$) = 0.43; PBO($d2$) = 0.22; PBO($d3$) = 0.10; PBO($d4$) = 0.06. Neglecting the small contribution of $d3$ and $d4$, the total bond orders will be:

$$8\,\mathrm{PBO}(d5) + 2\,\mathrm{PBO}(\mathrm{Cu-Cu}) = 5.76 \quad \text{for Cu}$$

and

$$4\,\mathrm{PBO}(d5) + \mathrm{PBO}(d1) + 2\,\mathrm{PBO}(d2) = 3.03 \quad \text{for Al.}$$

These remarkable values fit perfectly the 'valences' of 5.56 (Cu) and 3.00 (Al) assumed by Pauling to derive the single bond lengths. Furthermore, this simple treatment allows for more detailed analysis of the contributions of different interatomic interactions. In other words, both atoms are involved in heteroatomic as well as homoatomic interactions and the latter roughly corresponds to one additional Cu–Cu and one Al–Al bond per formula unit.

4.3. Periodic nodal surface (PNS) for description of the $CuAl_2$ structure

The periodic nodal surfaces (PNS) are symmetry governed space dividers [44] which are independent of any chemical structure. A simple Fourier series $R(\mathbf{r})$ is used for the calculation:

$$R(\mathbf{r}) = \sum_h |S(\mathbf{h})|k(\mathbf{h})\cos(2\pi\mathbf{hr} - \alpha(\mathbf{h})) = 0.$$

$S(\mathbf{h}) = \Sigma_i \delta_i \exp(2\pi i \mathbf{hr}_i)$ is the geometric structure factor; $k(\mathbf{h}) = (|\Phi_h|/|\mathbf{h}|)^2$ is a decay function; $\mathbf{h} = h\mathbf{a}^* + k\mathbf{b}^* + l\mathbf{c}^*$ and $\mathbf{r} = x\mathbf{a} + y\mathbf{b} + z\mathbf{c}$ are the vectors in reciprocal and direct space, respectively; $\alpha(\mathbf{h})$ is the phase shift of the $S(\mathbf{h})$ and of the symmetry related permutations. The relative values of the decay function $k(\mathbf{h}) \sim |\mathbf{h}|^{-2}$ reflect, e.g. the axial ratio c/a. They are included in the coefficients $S'(\mathbf{h}) = S(\mathbf{h}) \times k(\mathbf{h})$ and are normalized to unity for the shortest $\mathbf{h}$ vector $S'(\mathbf{h}_{\min}) = 1$ (according to (110) in case of $CuAl_2$). In general, only *one* or *two* factors $S(\mathbf{h})$ with the lowest order of $\mathbf{h}$ are necessary to represent the characteristic structural pattern in a given space group [45].

The reciprocal vectors (110), (200), (002) and (121) represent the lowest order of $\mathbf{h}$ for the $CuAl_2$ unit cell (space group $I4/mcm$; $c/a < 1$). But the first three reflect only the $I4/mmm$ symmetry corresponding to the non-characteristic special positions 4*a* and 8*h* of the space group $I4/mcm$. Therefore, the PNS calculated with $S(110)$ only shows a chessboard-like arrangement of square piles along [001]. The characteristic modulation (distortion) of these piles with respect to the full $I4/mcm$ symmetry is done by the coefficient $S(121)$ which is the lowest order reciprocal vector (121) containing the full symmetry of this space group. Note that the Al position 8*h* represents also the lowest multiplicity point configuration in direct space which contains the full space group symmetry [45].

The appropriate PNS $I4/mcm$ $\langle (110)_0^1; (121)_\pi^{0.2} \rangle$ $I4/mcm$ is shown in Fig. 2 (notation of PNS according [10]). The hyperbolic surface divides the space of the structure into two non-identical labyrinths. One of them (yellow) includes the complete polyhedral framework whereas the other (pink) seems to be 'empty'. The pink labyrinth renders well the shape of the *tetraedersterns* (Fig. 1, bottom) whose centers are located in this labyrinth. Furthermore, the PNS separates the regions of different chemical interactions (cf. Fig. 3 and further discussion).

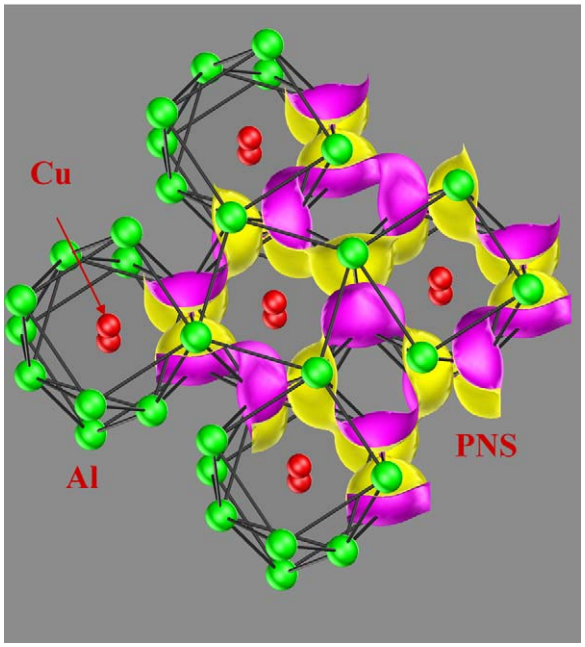

Fig. 2. Polyhedral representation of the structure of $CuAl_2$ and PNS $I4/mcm$ $\langle(110)_0^1;(121)_\pi^{0,2}\rangle I4/mcm$ flashing the 'empty' space between the columns of tetragonal antiprism.

4.4. Electron localization function and electron density in $CuAl_2$

In the ELF representation, each Al atom reveals two atomic shell basin sets [28] representing the 1st and 2nd atomic core shell. In the valence region aluminum (more precisely, the atomic shell basin set representing the 2nd atomic shell of Al) is surrounded by five basins. One of these basins (basin Ω_A) is (1Al + 1Al)-disynaptic (i.e. has common border with two core basins) and the attractor ($\eta = 0.80$) is located in the middle of the short Al–Al contact $d1$. This clearly represents an Al–Al two-center bond (Fig. 3, top left). The attractors ($\eta = 0.60$) of two further basins Ω_B are each located in the middle of the two longer Al–Al contacts $d2$ (Fig. 3, top right). However, a similar simple interpretation as for basin Ω_A is not possible for Ω_B as it is (2Al + 2Cu)-tetrasynaptic additionally sticking to Cu atoms of different neighboring SAP columns. For crystal chemical reasons it can be argued that it should more reflect an elongated Al–Al bond than an elongated Cu–Cu bond with d(Cu–Cu) = 4.29 Å. However, there exists no unique quantum mechanical procedure yet to decide on the relative importance of different neighbors of a basin. One possibility of

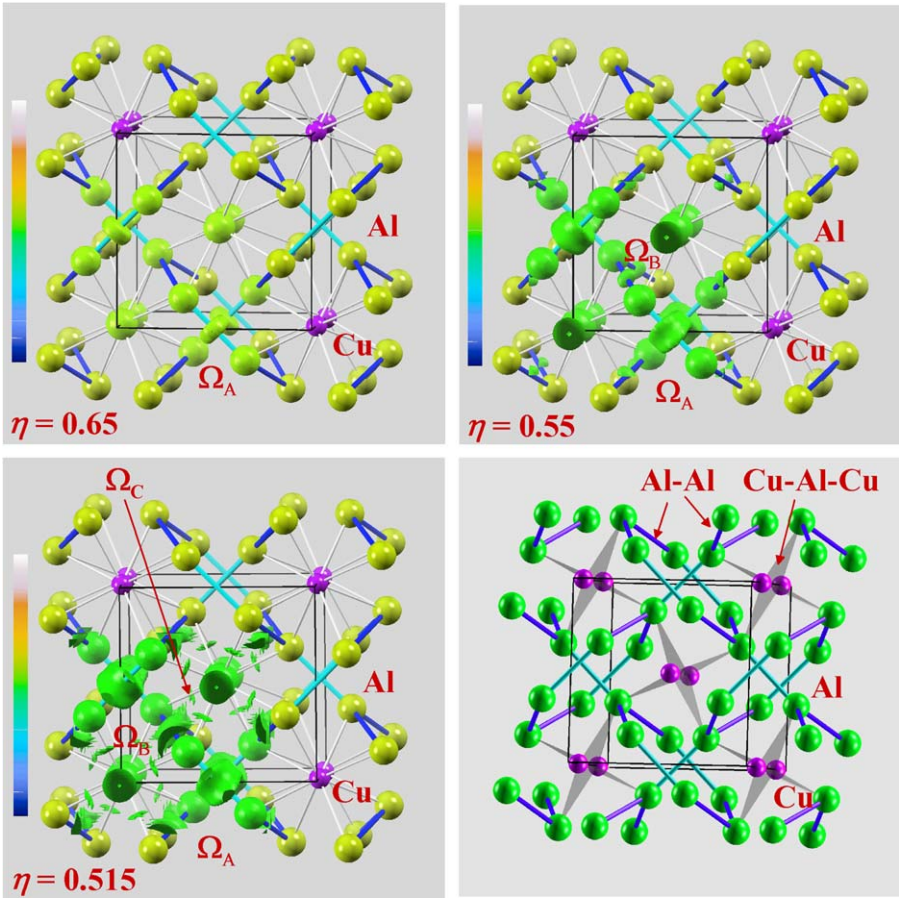

Fig. 3. View of the $CuAl_2$ structure along the [001] direction and isosurfaces of total ELF: *top left*—showing the two-center Al–Al bonds (basin Ω_A, $\eta = 0.65$, green); *top right*—two-center Al–Al bonds on the antiprism edges (basin Ω_B, $\eta = 0.55$); *bottom left*—three-center Cu–Al–Cu bonds (basin Ω_C, $\eta = 0.515$); *bottom right*—two- (dark and light blue) and three-center (gray) bonds in the $CuAl_2$ structure in the ELF representation.

investigation is the comparison between homonuclear dimer species Cu_2 (with d(Cu–Cu) = 4.29 Å) and Al_2 (with d(Al–Al) = $d2$). LDA calculations for different homonuclear species Cu_2^{2+}, Cu_2, Cu_2^{2-}, Al_2^{2+}, Al_2, Al_2^{2-} were carried out with the program ADF. From these calculations we can estimate a maximum value $\eta^{max} \leqslant 0.34$ between Cu atoms for those elongated Cu_2 species (occurring in the neutral dimer) and $\eta^{max} \geqslant 0.65$ for Al_2 species. The attractor value $\eta = 0.60$ occurring for basins Ω_B is much higher than the one expected for elongated Cu_2 species which indicates that the interaction $d2$(Al–Al) is the dominant one for the tetrasynaptic basin Ω_B. We therefore characterize basin Ω_B as representing primarily an elongated bond $d2$(Al–Al). The "coordination" of aluminum is completed by two (1Al + 2Cu)-trisynaptic basins Ω_C, whose attractors ($\eta = 0.53$) are each located within triangles Cu–Al–Cu of base-condensed SAPs running along [001] direction. Alternatively we may describe them occurring on the backside of the short Al–Al contact $d1$. So just from the location of the attractors there is an ambiguity in the interpretation: in the former description they are interpreted as Cu–Al–Cu three-center bonds, while in the latter they represent Al lone pair regions. In order to distinguish between these two alternatives we consider dimeric species Al_2 but now with a distance $d1 = 2.72$ Å, which is quite close to the distance established for jet-cooled Al_2 molecules ($d = 2.701$ Å) [46]. The electronic structure of the molecules Al_2^{2+}, Al_2 and Al_2^{2-} can be characterized as follows: Al_2 being a spin triplet molecule with an $s\sigma^2$, $s\sigma^{*2}$, $p\sigma^1$, $p\pi^1$ MO occupation (i.e. half of a $p\sigma$ and half of $p\pi$ bond) [46], Al_2^{2+} is a spin singlet with $s\sigma^2$, $s\sigma^{*2}$ MO occupation (i.e. Al–Al nonbonding) and Al_2^{2-} is a spin singlet with $s\sigma^2$, $s\sigma^{*2}$, $p\pi^4$ MO occupation (i.e. π double bonding without σ bonding, isoelectronic with C_2). For all these molecules the lone pair attractor value is not below $\eta = 0.8$, which is significantly larger than $\eta^{max} = 0.53$ observed for basin Ω_C. From this finding we can conclude that Cu atoms definitely have a large influence on basin Ω_C, which clearly points to the interpretation as a Cu–Al–Cu three-center bond.

Summarizing the results obtained by topological analysis of ELF we observe in the crystal structure of $CuAl_2$ only three different atomic interactions: clear Al–Al two-center bonding (basins Ω_A) along the contact $d1$, predominantly Al–Al-two-center bonding (basins Ω_B) along $d2$ with some multicenter bonding contributions and significant three-center bonding Cu–Al–Cu (basins Ω_C). These interactions were also observed in the FPLO calculation.

Further insight can be obtained integrating the total electron density in the valence basins. Our LMTO-ASA calculation results in electron counts of $q(\Omega_A) = 1.9\,e^-$, $q(\Omega_A) = 1.4\,e^-$ and $q(\Omega_C) = 0.8\,e^-$. From our CRYSTAL/TOPOND calculations with two different optimized basis sets we obtained $1.6\,e^-$ ($1.7\,e^-$) for Ω_A, $2.1\,e^-$ ($2.7\,e^-$) for Ω_B and $0.6\,e^-$ ($0.3\,e^-$) for Ω_C. The stronger varying basin populations for basins Ω_B and Ω_C are due to a flat $\eta(\mathbf{r})$ topology in that region, which results in very sensible basin boundaries between Ω_B and Ω_C (see also Section 3). Therefore, we cannot discuss the CRYSTAL/TOPOND basin populations. Counting the number of electrons per Al atom (LMTO-ASA results) involved in homonuclear Al–Al bonding gives $\frac{1}{2}q(\Omega_A) + 2*\frac{1}{2}q(\Omega_B) = 2.35\,e^-$, where we have neglected the Cu atoms participating at Ω_B. Thus, roughly two electrons per Al atom are involved in homonuclear σ bonding with 3 neighbors, which would result in a bond order of $\frac{2}{3}$ for each of the bonds in an undistorted 6^3 net. In the actual net, which corresponds to an orthorhombic distortion (plane group $c2mm$, $a' = a^{hex}\sqrt{3}$, $b' = a^{hex}$), the average bond order is about $\frac{2}{3}$ but it is composed of three bonds with bond orders 1 and $\frac{1}{2}$ in the ratio 1:2. A distortion from three equivalent $\frac{2}{3}$ bonds to 1 and $\frac{1}{2}$ bonds is expected to be energetically favored due to effects similar as for Peierls distorsion. However, we do not pursue this argumentation as the sheets cannot be considered isolated and Cu atoms play their role, too (see also Section 4.2): with the picture of distorted graphite sheets in mind, the chemical interpretation of heteronuclear interactions is straightforward. The two trisynaptic basins Ω_C per Al atom are located on opposite sides of the Al sheets, i.e. they have a π-like arrangement. This nicely accords with the electronic structure for Al_2 and Al_2^{2-} molecules mentioned above, which both have $p\pi$ bonding contributions. In contrast to this however, basins Ω_C are not (1Al–1Al)-disynaptic, as would be expected for π-bonding basins, but remain monosynaptic with respect to Al and stick each to 2 Cu atoms either above or below the sheet. This can be interpreted chemically either in the picture of a Lewis acid-base type of coordination or a bond formation from unsaturated fragments, both disrupting the initial Al–Al π-bond.

Considering the "coordination" of Cu outer core atomic shell basin set, each Cu atom is surrounded by 4 basins Ω_B and 8 basins Ω_C, which can be derived mathematically from the Al "coordination", too. There is no (1Cu + 1Cu)-disynaptic basin and no structuring of the outer core shell which implies that there is no participation of the outer core shell (i.e. 3d electrons) in chemical bonding for this compound. However, counting the number of electrons in the valence region gives $7.9\,e^-$ per formula unit (1 Ω_A + 2 Ω_B + 4 Ω_C) which is qualitatively similar to $8.2\,e^-$ from CRYSTAL/TOPOND (for both basis sets). Since each Al atom provides 2.9 electrons (i.e., $10.1\,e^-$ in Al core) each Cu atom must have provided 2.1 electrons in the valence region, which means, that the 3rd atomic shell basin set is not fully occupied but has an electronic population of $16.9\,e^-$. Qualitatively the same result is obtained from our CRYSTAL/TOPOND calculations. In view of *TM–TM* interactions (*TM* = transition metal) [28] this is a new feature. For those interactions treated therein the observed features of ELF were (i) an attractor between the metal atoms in the valence region, (ii) an increased electronic population of the valence shell, due to a participation of the 3rd atomic shell in chemical bonding, and (iii) a

structuring of the 3rd atomic shell. In the case of $CuAl_2$ we find the former two features but no structuring of the outer core shell. This is an indication that the 3rd atomic shell does not participate in chemical bonding. Instead, an electron is transferred into the valence region. This is fully consistent with results from Walch et al. [47], who showed on the basis of ab initio singles plus doubles configuration interaction (SDCI) and coupled pair functional (CPF) calculations on Cu_2 and Cu_3 molecules that, as soon as more than one bonding partner is present the $3d^9 4s^2$ configuration is strongly mixed into the initial $3d^{10}4s^1$ atomic ground state in order to achieve more favorable bonding interactions since Cu(3*d*) states are too contracted. Thus, in this case the lack of about one electron in the 3rd shell basin set is an indication for covalent interaction in the valence region mediated by the the 4th shell of Cu. According to our ELF analysis on crystalline $CuAl_2$ these interactions are Cu–Al–Cu three-center-bonds represented by trisynaptic basins Ω_C (see above). This interpretation is also supported by our COHP analysis (see next section), where the Cu–Al interaction is due to Cu(4*s*,*p*)–Al(3*s*,*p*) interactions and Cu(3*d*) orbitals do not play a significant role.

Having obtained electronic basin populations, it is now tempting to go one step further and assign atomic charges. This can be done, however, it must be kept in mind that there is (yet) no accepted biunique correspondence between the true charge (if it exists at all) of an atom in a chemical aggregate and any existing definition for that. Additionally, it is also no observable in the strict sense. Although there is no unbiased way to quantify charges this seems to be a common grain of truth in all different charge definitions [48]. Nevertheless the attribution of atomic charges and electronegativity scales is a part of strong chemical concepts. Thus we show that, for conceptual reasons, the atomic charge assignment is possible on the basis of quantum mechanical data even for intermetallic compounds. Using the partitioning of space by ELF basins, problems arise on (i) how to assign valence basins to atoms (for which one possible definition is given by the use of the synapticity) and, (ii) how to distribute the electronic population of a polysynaptic basin between its synaptic member atoms. In view of our discussion above we may assign basin $\frac{1}{2}$(1Al−1Al)-Ω_A's and either $2*\frac{1}{2}$ (neglecting the participation of 2 Cu atoms) or $2*\frac{1}{4}$(2Al+2Cu)-Ω_B's population to Al giving 2.35 electrons or 1.65 electrons, respectively. For basins Ω_C which represent three-center-bonding we equally distribute the charge among 2 Cu and 1 Al resulting in total electronic populations of either 2.88 e^- (from 2.35 $e^- + 2*\frac{1}{3}$ $q(\Omega_C)$) or 2.18 e^- (from 1.65 $e^- + 2*\frac{1}{3}$ $q(\Omega_C)$) for Al (see Fig. 4). Another possibility for the definition of an atomic charge using a direct space quantity is the traditional atoms in molecules (AIM) analysis according to Bader [26] which was applied for this purpose to $CuAl_2$. Within this method the charge assignment is uniquely defined, because space is completely divided into atomic basins and, besides some very rare cases, no extra

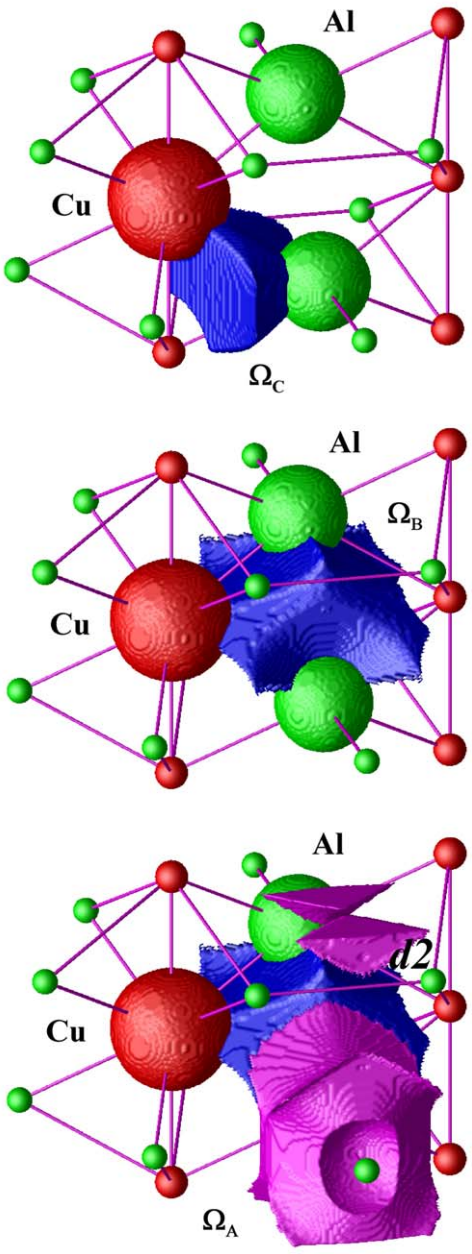

Fig. 4. ELF basins for inner atomic shells of copper (red) and aluminum (green), as well as for the bonds *d*1 (basin Ω_A, pink), *d*2 (basin Ω_B, blue) and Cu–Al–Cu (basin Ω_C, blue).

basins appear. The calculated electron density (Fig. 5, top) shows maxima on the atomic positions and very tiny maxima along the short contact *d*1. This occurrence of a non-nuclear maximum and a corresponding non-nuclear basin (NNB) is an artefact of the method of calculation (i.e., ASA), since it is absent in the density calculated with CRYSTAL/TOPOND or FPLO. For our purpose here the atomic populations are not significantly changed due to the presence of the NNBs with $q = 0.28\,e^-$: integration of the electron density within the atomic basins results in 12.1 e^- (LMTO-ASA, leaving NNBs unattributed), 12.2 e^- (LMTO-ASA, equally distributing the charge of NNBs between neighboring atomic basins) and 12.2 e^-

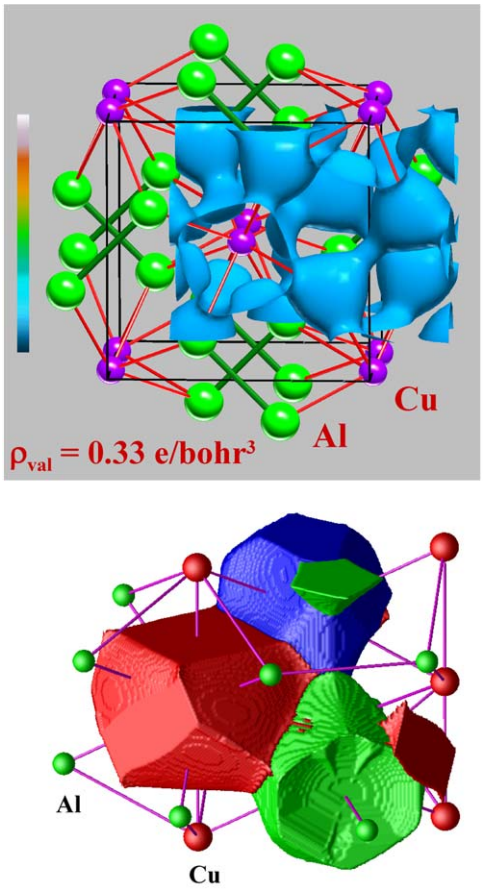

Fig. 5. Electron density in $CuAl_2$: *top*—isosurface of the valence electron density; *bottom*—Bader's atoms for copper (red) and aluminum (green and blue).

(CRYSTAL/TOPOND) for Al atoms. The resulting charge assignment ($Cu^{1.6-}$, $Al^{0.8+}$) is qualitatively in accord with both assignments using ELF partitioning. With view on traditional chemical concepts this charge assignment accords with the qualitative electronegativity difference between Cu and Al (e.g., 1.8 and 1.5, respectively, on the Allred-Rochow scale). Although this rules out the charge assignment given by Dehlinger et al. [49] assuming an eight-electron molecule Al_2^{2-}, we may note that they were correctly assuming 8 valence electrons per formula unit.

4.5. COHP analysis

Starting with homoatomic Al–Al interactions the different contacts along *d*1 and *d*2 are clearly differentiated in the COHP picture, too (Fig. 6). Sizable covalent interactions involving Al(3*s*3*p*) orbitals can be figured out for both contacts, where the larger ones—indicated by a larger value of integrated COHP (ICOHP)—are observed for the shorter contact (Fig. 6). The ratio ICOHP(E_F, *d*1)/ICOHP(E_F, *d*2) = −1.11 eV cell^{-1}/−0.67 eV cell^{-1} = 1.65 correlates with the corresponding ratio PBO(*d*1)/PBO(*d*2) = 1.95 (see Section 4.2) and with ELF analysis (if BO is defined as one half of the according basin

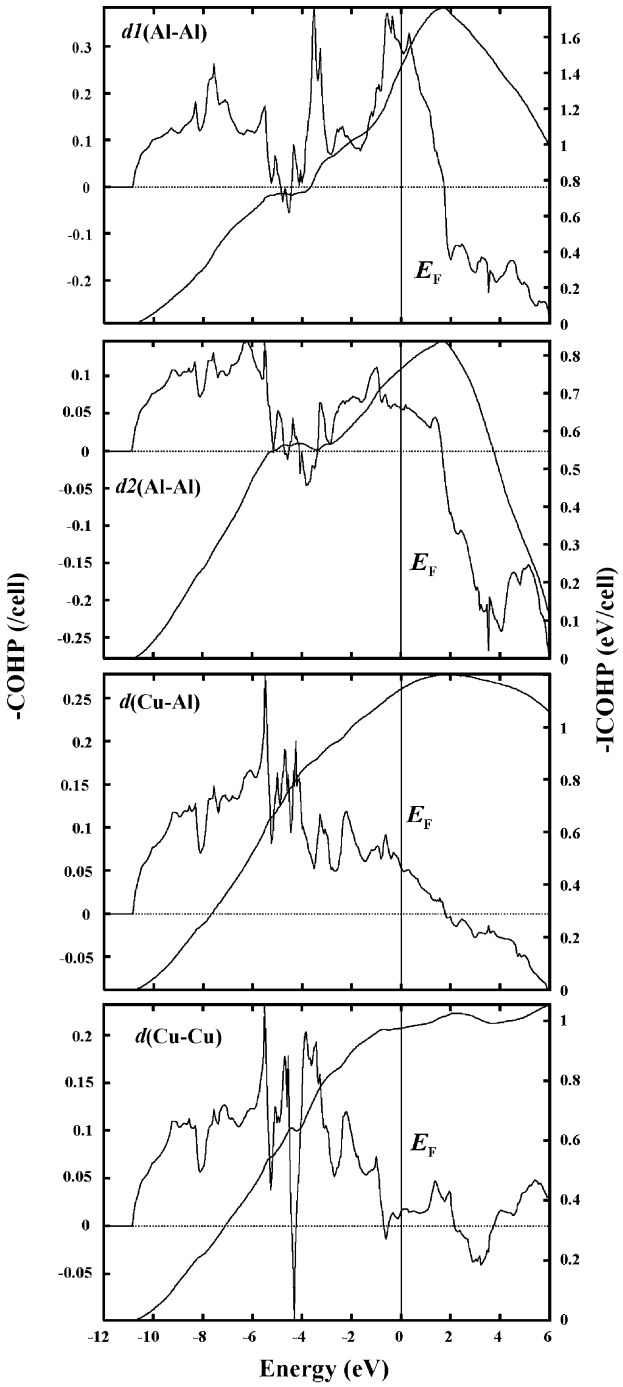

Fig. 6. COHP analysis of the interatomic interactions in $CuAl_2$.

population, than BO(*d*1)/BO(*d*2) = 0.95/0.7 = 1.36). A comparison of the COHP(*E*) around E_F shows a remarkable difference compared with the bonding situation in Zintl compounds: while for homoatomic bonding these interactions normally are saturated at E_F, for both interactions *d*1, *d*2 the virtual bonding interaction increases up to 4 eV beyond E_F. The maximum of both ICOHP(*E*, *d*1), ICOHP(*E*, *d*2) is at the same energy, and, additionally the sizable ICOHP(E, Al–Cu) for interactions Al–Cu is maximized there, too. It can be concluded that covalent

Al–Cu interactions are mediated at least partially by the same orbitals which are responsible for homoatomic Al–Al bonding. Weak homoatomic Cu–Cu interaction can be detected in the corresponding COHP(E) diagrams. However, they are not mediated by d–d interactions, which are characterized by completely occupied bonding/antibonding σ and π interactions below E_F. Within the framework of the method they are described as bonding Cu(4s4p)–Cu(4s4p) interactions. Similarly, Cu–Al bonding is achieved via Cu(4s,4p)–Al(3s,3p) interactions. Thus, the Cu(3d) electrons are not involved in bonding which perfectly agrees with analysis of ELF topology in the outer core region of Cu. The Cu orbital contributions to ICOHP($\leqslant E_F$, Cu–Cu) and ICOHP($\leqslant E_F$, Cu–Al) come from 4s, 4p orbitals. However for formally 4th shell orbitals of copper, which are quite diffuse (especially 4p), a method-inherent ambiguity exists between these orbitals and those which are Al-centered. Thus, part of the Cu–Cu orbital interaction described by COHP might be intermixed with Cu–Al interaction, which is in the same energy region. This would be the picture that ELF analysis is pointing at (three-center bonds Cu–Al–Cu).

4.6. Raman spectrum of $CuAl_2$

The Raman vibration spectra of the intermetallic compound $CuAl_2$ obtained are presented in Fig. 7. In order to assign the observed frequencies to distinct modes in the structure, the factor group analysis has to be done.

The structure of $CuAl_2$ contains six atoms in the primitive cell. According to group theory these give rise to 18 vibrations ($\Gamma = A_{1g}+2A_{2g}+2A_{2u}+B_{1g}+B_{2g}+B_{1u}+2E_g+3E_u$). Of these modes, the A_{1g}, B_{1g}, B_{2g}, and two E_g modes are Raman active, so a total of five modes are expected in the measurements [50].

Since the point group $mm2$ is not a maximal subgroup of the factor group $4/mmm$, the correlation table is not straight forward but takes a detour via the point group mmm [51,52]. Concerning the displacements of the atoms during the vibrations, it must be taken into account, that the orientation of the coordinate systems in the point and the space group are different. The atomic displacements for the Raman active modes are shown in Fig. 8.

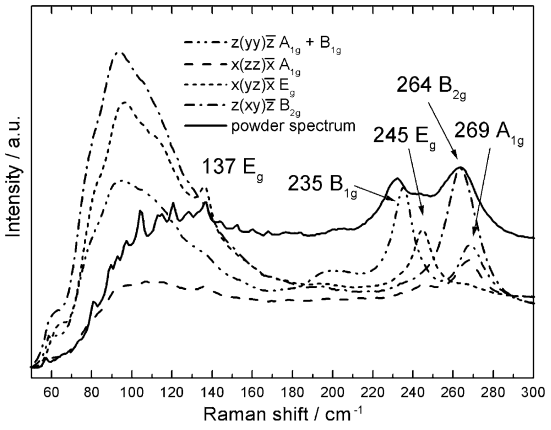

Fig. 7. Polarized Raman spectra of $CuAl_2$. The polarization direction and the direction of the incident and scattered light of the different experiments are given in Porto's notation [50].

The expected five modes (see above) are found in the experiment. A unique mode assignment was done from polarization measurements (Fig. 7). The eigenvectors of the highest frequency modes A_{1g} and B_{2g} correspond to $d1$(Al–Al) stretching vibration. Their nearly identical frequency values (Table 3) suggest almost independent vibration of the neighboring Al_2 dumb-bells within the (001) plane. Both are well compatible with the frequency of 297.5 cm^{-1} measured for Al_2 molecules in the $^3\Pi_u$ state in an argon matrix at 15 K [53] and with the value of 285.8 cm^{-1} measured for jet-cooled Al_2 molecules with d(Al–Al) = 2.701 Å [46]. Due to the limited amount of experimental information, only simple lattice dynamical models could be set up. Not all the models presented hereafter were dynamically stable. Especially two of them (models 1 and 3) displayed one unstable acoustic phonon branch. We include them however for demonstration, as further interaction parameters or even model 2 can cure that behavior. The simplest model (model 1) included three longitudinal force constants corresponding to the $d1$, $d2$ and d(Cu–Al) interactions (Table 4). As a next step, one additional transverse force constant was added into the fitting (model 2). The starting longitudinal components were obtained by fitting with the program VIBRATZ [54], the transverse components were added by variation with the UNISOFT program [55]. Already the three-parameter model allowed a fully acceptable fit of the experimental vibration frequencies (Table 4). Inclusion of the transverse force constants into four-parameter models improved the fit but did not substantially change the longitudinal components.

This suggests that the obtained fit parameters from model 2 can already be ascribed some physical relevance. The force constant for the Cu–Al interaction is quite independent of the model and significant. The harmonic force constants evaluated from the vibrational frequencies taken from Fu et al. [46] and Fang et al. [53] are 0.65 and 0.70 N cm^{-1}, respectively.

The according values for longitudinal components of $d1$ and $d2$ interactions are significantly smaller (Table 4). This correlates with the reduced bond orders from ELF analysis (0.95 for $d1$ and 0.7 for $d2$). The according experimental bond order values were calculated as a ratio of the force constants from the model 2 and the force constant from Fu et al. [46] in assumption of their proportionality to the bond order ratio [51] and resulted in $0.371/0.65 = 0.57$ and $0.154/0.65 = 0.24$ for $d1$ and $d2$, respectively. The difference between bond orders from experiment, structure data, ELF analysis and COHP obviously may originate from the evaluation procedures, but the trend is the same. On the other hand, we can re-calculate the bond distances applying Pauling's bond order—bond length equation [43], taking in account the single-bond distance of 2.70 Å

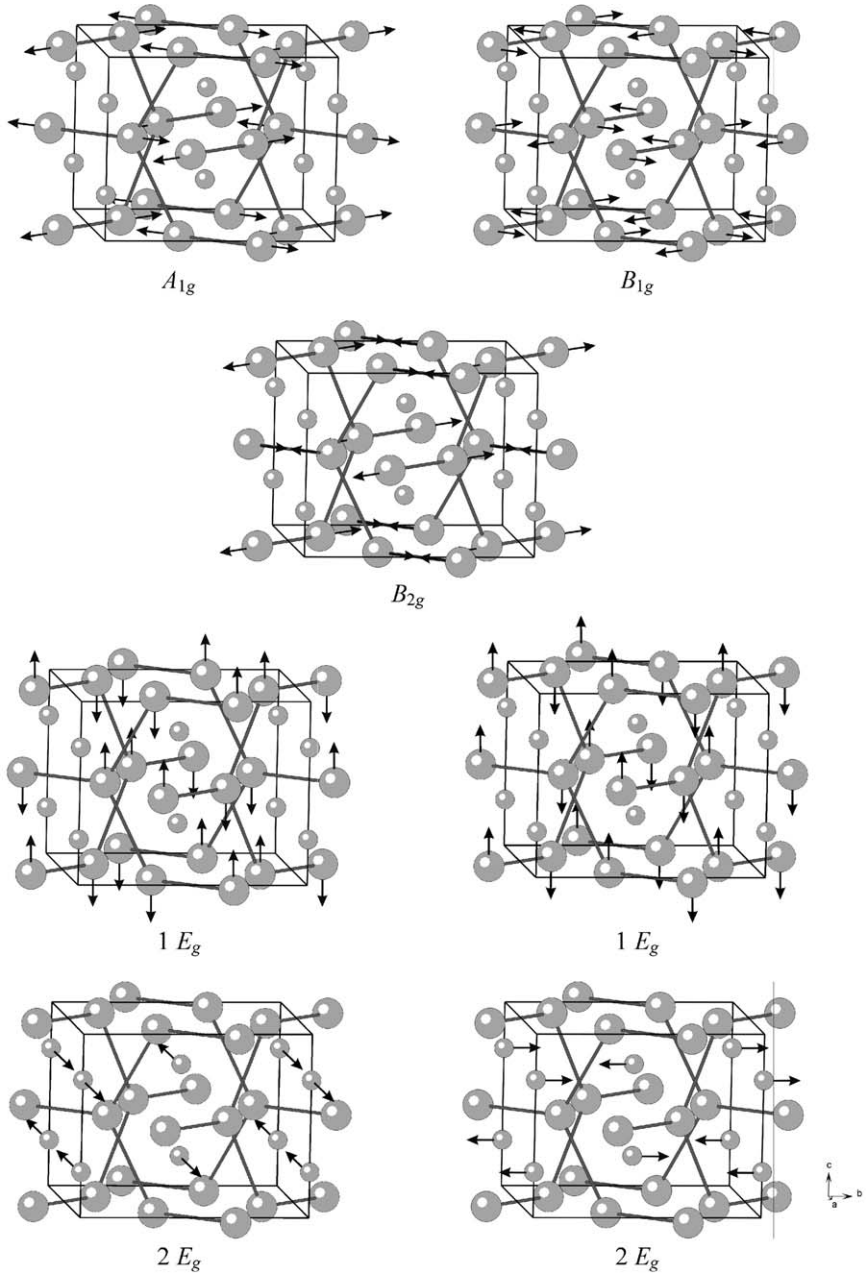

Fig. 8. Schematic drawing of the atomic displacements in the different Raman active modes. The real displacement of the atoms in the two E_g modes is a mixture of the displacements in $1E_g$ and $2E_g$.

Table 3
Measured and calculated Raman vibration frequencies (in cm^{-1}) for $CuAl_2$

Mode	Observed	Model 1 (VIBRATZ/ UNISOFT)	Model 2	Model 3
A_{1g}	269	266/265	267	267
B_{1g}	235	232/231	235	235
B_{2g}	264	266/265	267	267
E_g	245	252/251	245	245
E_g	137	124/123	137	137

found from Raman measurement [46] and bond orders from ELF analysis. This gives value $d1' = 2.715$ Å and $d2' = 2.810$ Å which is in good agreement with experimental values of $d1 = 2.7201$ Å and $d2 = 2.8975$ Å from the structure data.

4.7. High-pressure X-ray diffraction study

The bonding picture form the ELF representation is supported additionally by the results of high-pressure X-ray diffraction experiments on powder of $CuAl_2$. Whereas the unit cell volume behaves according to the

Table 4
Force constants (in $N\,cm^{-1}$) from different lattice dynamical models for $CuAl_2$

Model	No. of parameters	σ[a]	f_L(Cu–Al)	f_T(Cu–Al)	$f_L(d1)$	$f_L(d2)$	f_T(Cu–Cu)
1	3	3.64	0.312	—	0.389	0.198	—
2	4	0.81	0.3095	0.0275	0.371	0.154	—
3	4	0.81	0.322	—	0.429	0.138	0.095

[a]Average deviation for five Raman vibration frequencies (in cm^{-1}).

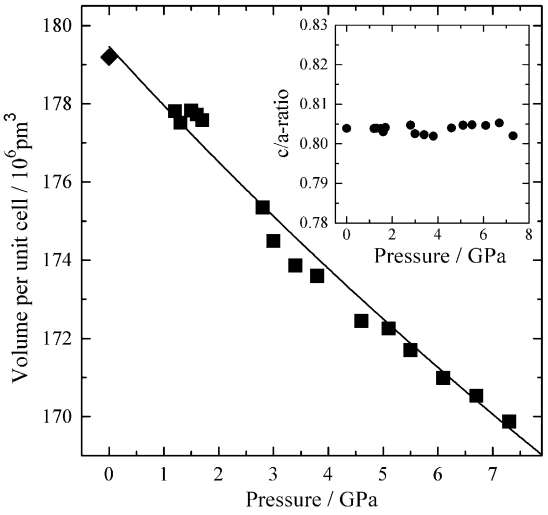

Fig. 9. Pressure dependence of the volume and the c/a ratio in $CuAl_2$. The change of the volume was fitted with an inverse Murnaghan equation: $V_0 = 179.5(6)$ Å^3, $B_0 = 117(13)$ GPa and B' set to 4. The statistical analysis of the scatter of the data implies a relative error of 0.3% and 0.2% for the volume and the c/a ratio, respectively.

expectation (Fig. 9), the c/a ratio for the tetragonal unit cell of $CuAl_2$ is astonishingly pressure-independent between ambient pressure and 11 GPa. This result correlates well with the picture of interpenetrating graphite-like nets suggesting nearly isotropical compressibility of the structure, because both lattice parameters a and c are mostly controlled by the Al–Al interactions within the graphite-like nets. In contrary, the polyhedral description of the $CuAl_2$ structure with piles of SAPs along [001] implies, in first row, the interaction between the central atom and the ligands, the Cu–Al interaction, and thus suggests more anisotropic compressibility according to the tetragonal symmetry.

5. Conclusions

The analysis of the bonding in the intermetallic compound $CuAl_2$ applying electron localization function combined with electron density leads to a new picture of chemical interaction in this structure. The three-bonded aluminum atoms form interpenetrating graphite-like nets by two-center bonds. Each copper atom is located in the tetragonal antiprismatic cavity of this network and is bounded to the aluminum environment by eight three-center bonds. This constellation requires one d electron of copper to participate in the bonding in the valence region. Among different ways for describing the $CuAl_2$ structure which can be found in literature from the analysis of geometrical characteristics, the quantum-chemical investigation favors a combined picture with three decisive interactions: two different intra-network Al–Al bonds and additional Cu–Al–Cu interaction. The polarized Raman investigations and high-pressure X-ray powder diffraction experiments support the bonding picture from ELF representation. The question, how far the bonding properties obtained for $CuAl_2$ can be generalized to other representatives of this structure type, is under investigation [52] and will be addressed elsewhere.

Acknowledgments

We acknowledge the European Synchrotron Radiation Facility for provision of synchrotron radiation facilities and we would like to thank M. Hanfland for assistance in using beamline ID09.

References

[1] J.B. Friauf, J. Am. Chem. Soc. 49 (1927) 3107–3114.
[2] P.I. Kripiakevich, Structure Types of Intermetallic Compounds, Nauka, Moscow, 1977 (in Russian).
[3] K. Schubert, Kristallstrukturen zweikomponentiger Phasen, Springer, Berlin, Göttingen, Heidelberg, 1964.
[4] W.B. Pearson, The Crystal Chemistry and Physics of Metals and Alloys, Wiley-Interscience, New York, London, Sydney, Toronto, 1972.
[5] H. Nowotny, K. Schubert, Z. Metallkd. 37 (1946) 17–23.
[6] B.G. Hyde, S. Andersson, Inorganic Crystal Structures, Wiley, New York, 1989.
[7] U. Häußermann, S. Lidin, J. Solid State Chem. 132 (1997) 151–155.
[8] U. Häußermann, S. Lidin, J. Solid State Chem. 134 (1997) 431.
[9] A.E. Dunsworth, J.-P. Pan, H.L. Skriver, J. Phys. F. Metal Phys. 9 (1979) 1077–1084.
[10] Y. Grin, U. Wedig, F. Wagner, H.G. von Schnering, A. Savin, J. Alloys Compd. 255 (1997) 203–208.
[11] L. G. Akselrud, Yu. Grin, V. K. Pecharsky, P. Zavalij, WinCSD, version 10.2005, 2005.
[12] G.M. Sheldrick, SHELXL-97, release 97-2, WinGX version, 1997.
[13] T.C. Damen, S.P.S. Porto, B. Tell, Phys. Rev. 142 (1966) 570–574.
[14] G.J. Piermarini, S. Block, J.D. Barnett, R.A. Forman, J. Appl. Phys. 46 (1975) 2774–2780.
[15] H.K. Mao, P.M. Bell, J.W. Shaner, D.J. Steinberg, J. Appl. Phys. 49 (1978) 3276–3283.
[16] A.P. Hammersley, S.O. Svensson, M. Hanfland, A.N. Fitch, D. Häusermann, High Press. Res. 14 (1996) 235–248.

[17] O. Jepsen, A. Burkhardt, O.K. Andersen, The Program TB-LMTO-ASA, version 4.7, Max-Planck-Institut für Festkörperforschung, Stuttgart, 1999.
[18] U. Barth, L. Hedin, J. Phys. C 5 (1972) 1629.
[19] O.K. Andersen, Phys. Rev. B 12 (1975) 3060.
[20] W.R.L. Lamprecht, O.K. Andersen, Phys. Rev. B 34 (1986) 2439.
[21] R. Dronskowski, P.E. Blöchl, J. Phys. Chem. 97 (1993) 8617–8624.
[22] F. Boucher, O. Jepsen, O.K. Andersen, Supplement to the TB-LMTO-ASA V4.7 Program, Stuttgart, Germany.
[23] A.D. Becke, K.E. Edgecombe, J. Chem. Phys. 92 (1990) 5397–5403.
[24] A. Savin, H.J. Flad, J. Flad, H. Preuss, H.G. von Schnering, Angew. Chem. 104 (1992) 185;
A. Savin, H.J. Flad, J. Flad, H. Preuss, H.G. von Schnering, Angew. Chem. Int. Ed. Engl. 31 (1992) 185.
[25] A. Savin, O. Jepsen, J. Flad, O.K. Andersen, H. Preuß, H.G. von Schnering, Angew. Chem. 104 (1992) 186–188;
A. Savin, O. Jepsen, J. Flad, O.K. Andersen, H. Preuß, H.G. von Schnering, Angew. Chem. Int. Ed. Engl. 31 (1992) 187.
[26] R.F.W. Bader, Atoms in Molecules: A Quantum Theory, Oxford University Press, Oxford, 1990.
[27] B. Silvi, A. Savin, Nature 371 (1994) 683–686.
[28] M. Kohout, F.R. Wagner, Yu. Grin, Theor. Chem. Acc. 108 (2002) 150–156.
[29] For more details see http://www.cpfs.mpg.de/ELF.
[30] C. Gatti, TOPOND98 User's Manual, CNR-CSRSRC, Milano, 1999.
[31] R. Dovesi, V. R. Saunders, C. Roetti, M. Causa, N. M. Harrison, R. Orlando, C. M. Zicovich-Wilson, CRYSTAL98 User's Manual, University of Torino, 1998.
[32] K. Koepernik, H. Eschrig, Phys. Rev. B 59 (1999) 1743.
[33] A. Ormeci, H. Rosner, F.R. Wagner, M. Kohout, Yu. Grin, J. Phys. Chem. A 110 (3) (2006) 1100.
[34] M. Kohout, Program DGrid, version 2.3, Max-Planck-Institut für Chemische Physik fester Stoffe, Dresden, 2003.
[35] ADF2002.03, SCM, Theoretical Chemistry, Vrije University, Amsterdam, The Netherlands, http://www.scm.com.
[36] M. Kohout, Basin, version 2.3, Max-Planck-Institut für Chemische Physik fester Stoffe, Dresden, 2001.
[37] B. Silvi, J. Mol. Struct. 614 (2002) 3–10.
[38] C. Wolverton, V. Ozoliņš, Phys. Rev. Lett. 86 (2001) 5518–5521.
[39] D. Stockdale, J. Inst. Metals 52 (1933) 111–118.
[40] T. Gödecke, F. Sommer, Z. Metallkde. 87 (1996) 581–586.
[41] A. Meetsma, J.L. de Boer, S. van Smaalen, J. Solid State Chem. 83 (1989) 370–372.
[42] F. Haarmann, M. Armbrüster, Yu. Grin, J. Am. Chem. Soc. (2006), submitted.
[43] L. Pauling, The Nature of the Chemical Bond and the Structure of Molecules and Crystals, third ed., Cornell University Press, Ithaca, New York, 1960.
[44] H.G. von Schnering, R. Nesper, Z. Phys. B Condens. Matter 83 (1991) 407.
[45] T. Hahn, A. J. C. Wilson, International Tables for Crystallography, Volume A, fourth revised ed., Kluwer Academic Publishers, Dordrecht, Boston, London, 1996 (chapter 14).
[46] Z. Fu, G.W. Lemire, G.A. Bishea, M.D. Morse, J. Chem. Phys. 93 (1990) 8420–8441.
[47] S.P. Walch, C.W. Bauschlicher, S.R. Langhoff, J. Chem. Phys. 85 (1986) 5900–5907.
[48] J. Meister, W.H.E. Schwarz, J. Phys. Chem. 98 (1994) 8245–8252.
[49] U. Dehlinger, Z. Elektrochem. 41 (1935) 344–346.
[50] D.L. Rousseau, R.P. Bauman, S.P.S. Porto, J. Raman Spectros. 10 (1981) 253–290.
[51] J. Weidlein, U. Müller, K. Dehnicke, Schwingungsspektroskopie, 2. überarbeitete Auflage, Thieme, Stuttgart, 1988.
[52] M. Armbrüster, Bindungsmodelle für intermetallische Verbindungen mit der Struktur des $CuAl_2$-Typs. Dissertation, TU Dresden, 2004.
[53] L. Fang, B.L. Davis, H. Lu, J.R. Lombardi, Spectrochim. Acta A 57 (2001) 2809–2812.
[54] E. Dowty, VIBRATZ for Windows, version 1.21, Shape Software, 2002.
[55] P. Elter, G. Eckold, Physica B 276–278 (2000) 268–269.